Food Eng Rev (2016) 8:306–322
DOI 10.1007/s12393-015-9137-8

REVIEW ARTICLE

Evaluation of Food Quality and Safety with Hyperspectral Imaging (HSI)

Raúl Siche[1] · Ricardo Vejarano[1] · Victor Aredo[1] · Lia Velasquez[1] · Erick Saldaña[2] · Roberto Quevedo[3]

Received: 27 July 2015 / Accepted: 8 November 2015 / Published online: 23 November 2015

Abstract The current lifestyle and a greater awareness of the benefits of proper nutrition demand requirements for products offered in the market, being very important the safety, sensory attributes and composition of these respect to the benefits from their constituents, which in most of cases can only be assessed using techniques that require high investment of human, technological and time resources. This has caused the food industry to seek to develop products, besides the aforementioned requirements, which use technologies with less product loss during the analysis. Of all the available options, hyperspectral imaging technology is shown as one of the most promising alternatives, being a nondestructive analysis technology that can easily engage in productive processes. In this review, we collect the most important studies conducted using the hyperspectral imaging technology in assessing the quality and safety of food products, such as fruits and vegetables, legumes, cereals, meats, dairy and egg products.

Keywords Hyperspectral imaging · Spectral signature · Food analysis · Food quality and safety · Nondestructive

✉ Raúl Siche
rsiche@unitru.edu.pe

[1] Instituto Regional de Investigación Agraria, Facultad de Ciencias Agropecuarias, Universidad Nacional de Trujillo, Av. Juan Pablo II s/n. Ciudad Universitaria, Trujillo, Peru

[2] Department of Agro-industry, Food and Nutrition, "Luiz de Queiroz" Agricultural College, University of São Paulo, Piracicaba City, SP 13418-900, Brazil

[3] Food Science and Technology Department, Universidad de Los Lagos, Osorno, Chile

Introduction

The current food industry is focused on developing innocuous products that meet the quality requirements demanded by the market, but using technologies quick and accurate response [99], with less product loss during the analysis.

Of the many available technologies, hyperspectral imaging (HSI) is shown as a promising alternative, offering speed, accuracy, reliability, besides being a nondestructive analysis technology that can be attached along the different production processes [28], obtaining information immediately, something that other technologies cannot do.

To this must be added the efforts of the scientific community that directed significant research toward optimizing the adaptability of HSI to the food production processes, which is evidenced by the different studies published in the last decade (Fig. 1).

Figure 1 shows that from the year 2011 there have been a considerable increase in number of studies on the application of HSI in life sciences. This indicates that, as an alternative technology, the acceptance of HSI by industry was increasing, thanks to the advantages already mentioned above.

The objective of this review is to gather the most important studies conducted on the application of HSI in the evaluation of the quality and safety of food, referring first to the fundamentals of this analytical technology and then detailing its application to different food groups.

Fundamentals of Hyperspectral Imaging (HSI)

This technology had its origins between the 1970s and 1980s with the beginnings of the mineral mapping and the development of airborne imaging spectrometer (AIS) in identification works on surface of materials using remote

Table 1 Spectral images based on the spectral resolution [44]

	Multispectral	Superspectral	Hyperspectral	Ultraspectral
Spectral bands	1–10	10–100	100–1000	>1000
Spectral resolution ($\Delta\lambda$)	≈100 nm	≈50 nm	≈10 nm	≈1 nm

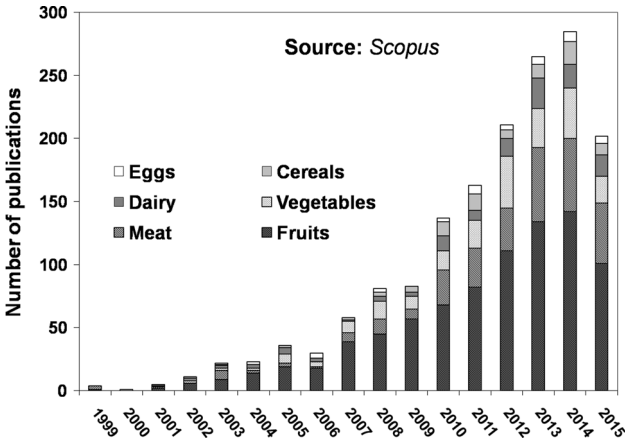

Fig. 1 Publications of scientific articles on the application of hyperspectral imaging (HSI) in the food industry. Information obtained from the database Scopus (search criteria: ALL FIELDS: "hyperspectral imaging" and ARTICLE TITLE, ABSTRACT, KEYWORDS: "each group of food")

sensing imagery conducted by the team Alexander Goetz at the California Institute of Technology [33].

Later, this technology showed its versatility to applications other than remote sensing, with applications in fields such as environment, geology, pharmaceutical industry [28], medical sciences [38] and food industry [50, 77, 96, 115].

Hyperspectral imaging, also called spectroscopic imaging or imaging spectrometry, is a powerful spectroscopic technique for nondestructive analysis that involves the acquisition of a stack of images of the same object at different spectral bands. The combined nature of the images and spectroscopy provides simultaneously physical and geometrical characteristics such as shape, size, appearance and color of the sample under analysis and the chemical composition thereof through spectral analysis [28, 122].

Besides the HSI, there are other kinds of spectral images: multi-, super- and ultraspectral [44], which are classified according to the number of bands and the spectral width of each band (Table 1). In all cases, the spectral image is a stack of images of the same object, each in a different spectral band. The smaller the width of each band, the better the spectral resolution, because reflectance continuous spectra are obtained.

Multispectral images consist of not more than ten spectral bands, while hyperspectral images contain hundreds of contiguous bands and regularly spaced. Therefore, hyperspectral images are a better source of information, providing a complete and broad spectrum in each pixel of the image [5].

All spatial characteristics of the samples under analysis can be viewed in different wavelengths (spectral dimension), so that an image can be analyzed in a single wavelength or by a combination of different wavelengths. No image on a single wavelength has sufficient information to fully describe a sample, which explains the advantage of HSI in food analysis because of the complexity of their structure and composition [28, 52].

During sample analysis, electromagnetic radiation incident on them generates spatial maps called hypercubes [28, 105, 106], obtaining three-dimensional databases comprising two spatial dimensions (x rows by y columns) and a spectral dimension (wavelength λ) (Fig. 2a).

Each hypercube consists of 50–300 images acquired at different wavelengths with a spectral resolution of 1–10 nm (Table 1). The basic criteria commonly applied to collect spectral information are: (a) the sequential acquisition of two-dimensional images at different wavelengths within a specific range of the spectrum, or (b) obtaining the full spectrum of each pixel of a line or area of an image at specific spectral region [66].

The basic principle of HSI is that all samples reflect, scatter, absorb and emit electromagnetic energy obtaining different patterns in specific wavelengths due to the difference in chemical composition and physical structure. For a constituent, if the percent reflectance is plotted against wavelength, the resulting curve is referred to as "spectral signature" or "fingerprint spectrum" of that constituent (Fig. 2b). Each component has a characteristic spectral signature reporting its chemical composition, which can be used to characterize, identify and discriminate between classes or types, in each pixel of the image [102]. Differences in the concentration of the chemical constituents of the sample have different reflectance values (or absorbance) in some key wave lengths. Figure 2b shows that the main constituents are totally different in terms of the reflectance values in the spectrum due to the different concentrations of chemical constituents such as water, proteins, fats that could have samples.

Evaluation of Food Through Hyperspectral Imaging

External attributes such as size, shape, color and surface texture can be easily evaluated by image analysis, but the prediction of parameters such as moisture content, fat or protein is difficult [23]. Spectroscopy alone is applicable in

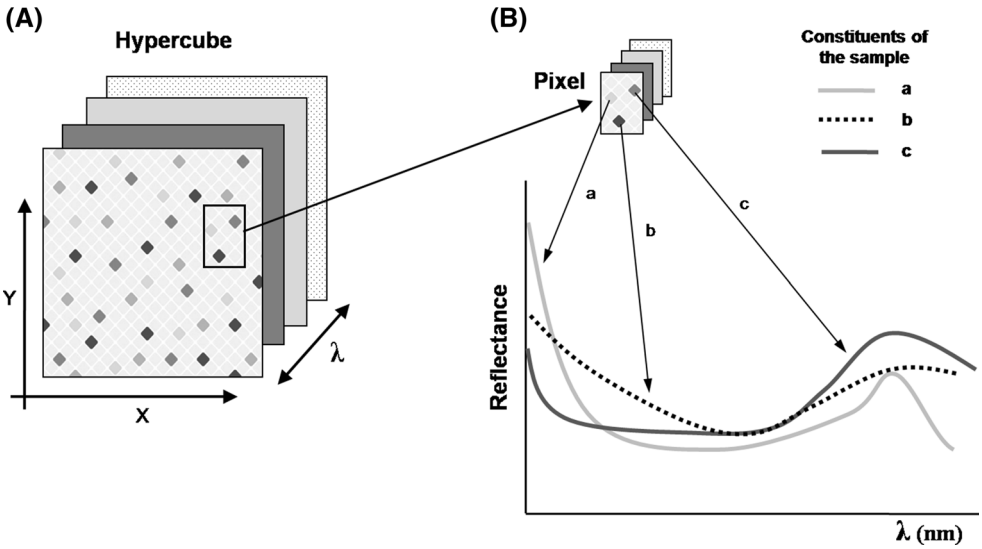

Fig. 2 **a** Hypercube representative pixel in a hyperspectral image. **b** Spectral signatures for each constituent of the sample (constituents: *a*, *b* and *c*)

the characterization of homogeneous materials, providing mean values of the sample properties. If the sample is heterogeneous in composition, different values depending on the location of the measurement are obtained. Indeed, this heterogeneity in the sample does not follow unless the spectroscopic measurement is repeated many times in a systematic way. This is inefficient in a practical application that must be controlled throughout the sample surface [76], besides involving greater investment of resources in the form of money, personnel and time.

It is also important to check the presence of extraneous agents which may represent a hazard to the consumer, which means ensuring food safety, so that these products do not cause any harm, either by adulteration, for the synthesis of harmful components as a result of deterioration, or by the presence of external contaminating agents [20, 31, 50, 55, 108].

In this sense, HSI has been applied in the evaluation of different types of food (Fig. 1); however, numerous investigations and optimization of their applications continue to be developed to adapt to a wider range of products. In this section, specific applications for different food groups in which this technology is used in both quality assessment and safety are described.

Fruits and Vegetables

In the food chain, fresh fruits and vegetables must undergo numerous processing steps, such as harvesting, cleaning, sorting, grading and packing before being shipped to markets. Throughout these steps, these are generally susceptible to extensive damage, which are not limited to mechanical damage but extend to pathogen invasion [67] or contamination by other external agents which may represent a hazard to consume.

Some damage is not easy to recognize by naked eye; moreover, the large number of fruits that pass through processing lines generates considerable difficulties that can lead to significant error during the inspection, which, if done manually, is expensive, inefficient, inconsistent and subject to human error.

The solution to this problem is to look for alternatives to help eliminate the disadvantages of traditional systems. Such defect detection systems must be fast, consistent, accurate and sensitive to detection of various defects from the onset of symptoms. Hyperspectral images have the potential to detect some defects automatically even before they are visible to the human eye [28].

The principle of applying the HSI in the evaluation of fruits and vegetables is the absorption of incident light, related to the chemical constitution of the sample, such as sugar content, while the light scattering is influenced by physical/structural characteristics such as the density, particle size and cell structure [94].

Numerous studies such as those shown in Table 2 have shown great potential in determining quality parameters and defect detection using different HSI acquisition modes and different ranges of wavelengths (λ) ranging from the visible spectrum to near infrared, all aimed at optimizing the application of this technology to fulfill quality requirements through automated inspection and implementation of classification systems that are fast, reliable, nondestructive and inexpensive. In this regard, HSI has a remarkable performance for estimating physical attributes such as strength, the presence of bruises and injuries, dry matter, soluble solids, pH.

Table 2 Some applications of HSI in assessing the quality and safety of fruits and vegetables

Product	Parameter	λ (nm)	Accuracy	References
Fruits				
Grape: red/white	Total phenols	950–1650	$R^2 = 0.89/0.80$	[77]
	°Brix	950–1650	$R^2 = 0.99/0.95$	[77]
	Titratable acidity	950–1650	$R^2 = 0.98/0.93$	[77]
	pH	950–1650	$R^2 = 0.94/0.94$	[77]
Red grape	Extractable total phenolic content	900–1700	$R^2 = 0.82$	[78]
	Extractable anthocyanin content	900–1700	$R^2 = 0.79$	[78]
	Anthocyanins content	900–1700	$R^2 = 0.94$	[12]
	Anthocyanins content	400–1000	$R^2 = 0.65$	[30]
	Discrimination between different grape varieties	950–1650	86 %	[79]
Strawberry	Detection of bruises	650–1000	90.7 %	[74]
	Moisture content, total soluble solids and pH	400–1000	$R = 0.87$, 0.80 and 0.92	[24]
Mango	Skin damage	650–1100	91.4 %	[114]
Apple	Detection of bruises	400–1000	94 %	[25]
	Detection of bruises	400–1000	86 %	[125]
	Detection of bruises	900–1700	94 %	[62]
	Firmness	500–1040	$R = 0.74$	[80]
	Firmness/soluble solids	450–1000	$R = 0.89/0.88$	[86]
	Firmness/soluble solids	500–1000	$R = 0.84/0.86$	[95]
	Chilling injury	400–1000	98.4 %	[26]
	Sugar content	685–900	$R = 0.91$	[135]
	Starch index	1000–1700	80.8 %	[69]
	Fecal contamination	400–1000	100 %	[54]
Peach	Firmness	500–1000	$R^2 = 0.58$ and 0.77	[63]
Orange	Soluble solids	700–1100	$R^2 = 0.96$ and 0.998	[59]
Banana	Soluble solids	400–1000	$R^2 = 0.85$	[98]
	Moisture	400–1000	$R^2 = 0.87$	[98]
	Firmness	400–1000	$R^2 = 0.91$	[98]
Vegetables				
Cucumbers	Detection of bruises	900–1700	82–93 %	[4]
	Internal defects	400–1000	99 %	[6]
	Chilling injury	447–951	93 %	[13]
	Chilling injury	447–951	90 %	[58]
Tomato	Firmness and ripeness	500–1000	$R = 0.66$	[94]
	Skin damage	1000–1700	96.4 %	[57]
Mushrooms	Chilling injury	400–1000	98 %	[35]
Spinach	*Escherichia coli* detection	400–1000	$R^2 = 0.97$	[109]
Onion	Detecting skin sour	950–1650	87 %	[116]
Potato	Prediction of cooking time	400–1000	$R^2 = 0.94$–0.96	[75]
Cabbage	Bacterial contamination	700–1100	$R = 0.95$	[110]

R correlation coefficient, R^2 coefficient of determination

An important aspect to consider in the quality of the fresh food is the outer appearance, which is the first attribute perceived by consumers when choosing them. This is why the control and selection of defective products is a vital task. For example, a lesion on the skin of foods carries the risk of contamination by pathogens [57]. The application of the HSI can be a valuable tool for detection of defective products as this may not possible by visual inspection, especially at an early stage. This would prevent future losses during distribution or sale of the product.

These defects are more common in products susceptible to mechanical damage, such as mango, whose mechanical damage to the skin were evaluated [114], obtaining better detection of skin damage in the range of 700–800 nm, with a rate of correct classification of 91.4 % (Fig. 3a). In similar studies developed to detect bruises by hyperspectral imaging in other products, Nagata et al. [74] at wavelengths in the range of 650–1000 nm identified 90.7 % bruises in strawberry using two key wavelengths (825 and 980 nm). In apples, various studies were carried out, as developed by ElMasry et al. [25], Lu [62] and Xing et al. [125], who obtained detection accuracies of 94, 94 and 86 %, respectively, as shown in Table 2.

Also, bruises in vegetables such as cucumbers were successfully detected by Ariana et al. [4]. Principal component analysis (PCA), band ratio and band difference were applied in the image processing to segregate bruised cucumbers from normal cucumbers. Best detection accuracies from the PCA were achieved when the spectral region was 950–1350 nm (95 %). The best band ratio of 988 and 1085 nm had detection accuracies between 93 and 82 %, whereas the best band difference of 1346 and 1425 nm had accuracies between 89 and 84 %. More recently, Lee et al. [57] evaluated the use of hyperspectral NIR reflectance imaging (1000–1700 nm) for detecting cuticle cracks on tomatoes, obtaining 96.4 % accuracy to classify tomatoes with and without crack defects.

Detection of other defects due to chilling injury, internal lesions, microbial contamination, among others, is another challenge which is considered as a critical issue as these defects can be the source for decay and microbial growth.

Regarding microbial contamination in fruits like apples, recently has been developed a hyperspectral system (fluorescence and reflectance imaging) to detect fecal spots on artificially contaminated apples, with a detection rate of 100 % by fluorescence imaging and 99.5 % by reflectance imaging [54]. Likewise, early detection of pathogenic contamination in packaged fresh vegetables can be useful

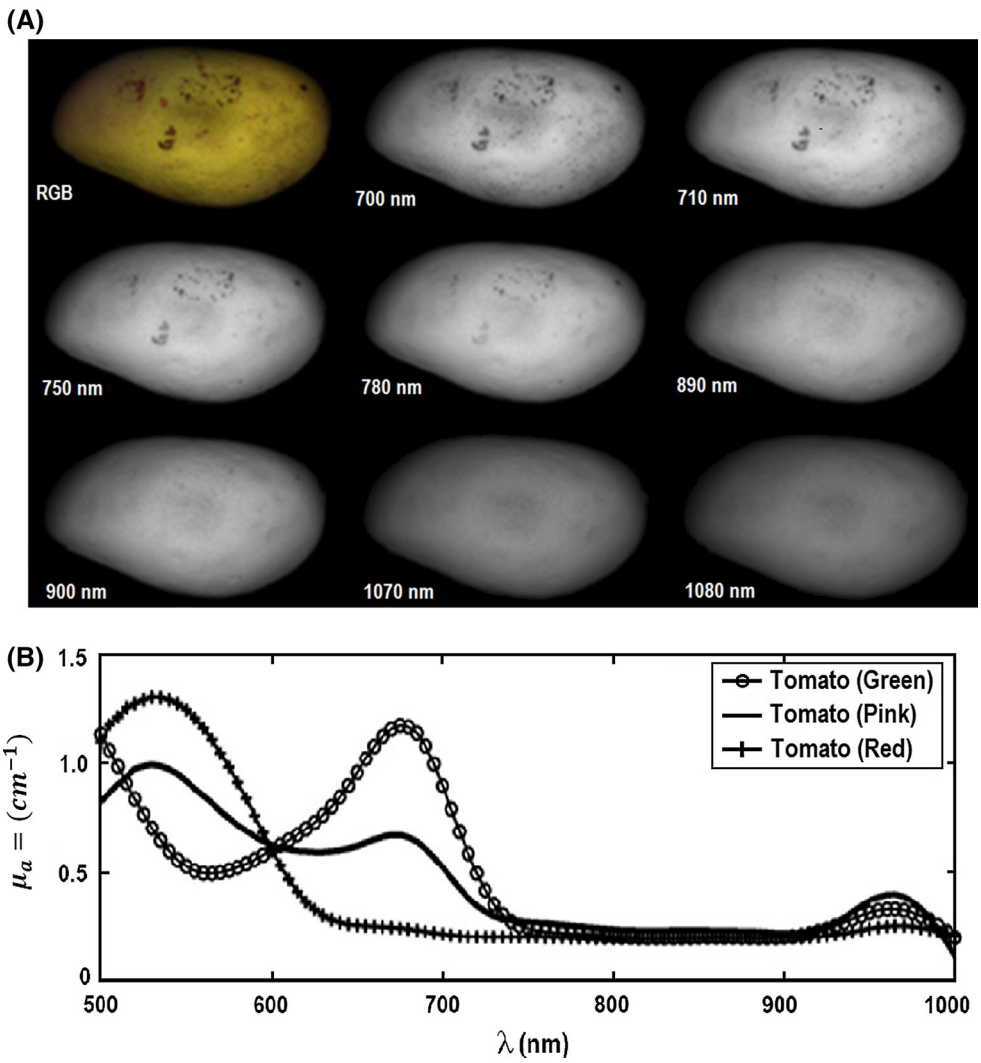

Fig. 3 **a** Images of mango skin damage captured at different wavelengths. RGB: image red, green, blue; adapted from Vélez et al. [114]. **b** Absorption spectrum of tomato in three different states: green, ripening fruit and mature; adapted from Qin and Lu [94]

to prevent the intake of contaminated products, as demonstrated Siripatrawan et al. [109], who evaluated the capability of hyperspectral imaging to detect the presence of *Escherichia coli* into packaged spinach samples, measured by a colony count (CFU) and a hyperspectroscopic technique at 400–1000 nm. The coefficient of determination obtained was $R^2 = 0.97$.

With respect to vegetables spoilage, "sour skin" (produced by *Burkholderia cepacia*) is a major postharvest disease for onions and causes substantial production and economic losses. A shortwave infrared hyperspectral reflectance imaging system was explored by Wang et al. [116] to detect sour skin (950–1650 nm), which discriminated 87 % healthy and sour skin-infected onions.

Chilling injury is a disorder manifested as a discoloration of the peel, color change in the pulp and the endocarp (seed coat), and cell disorganization and death in tissues, that may occur at any time due to harmful environmental conditions during the numerous processing steps such as harvesting, cleaning, sorting, grading and packing before being shipped to markets, or even in a home refrigerator. Several studies have been developed to classify different fruits to detect firmness changes due to chilling injury.

ElMasry et al. [26] applied hyperspectral imaging (400–1000 nm) for detecting chilling injury in apples, obtaining an average classification accuracy of 98.4 % for distinguishing between normal and injured apples. In other similar studies to detect chilling injured spots in cucumbers, Cheng et al. [13] and Liu et al. [58] obtained classification accuracies of 93 and 90 %, respectively, working at wavelength in the range of 447–951 nm. Meanwhile, Gowen et al. [35] used a pushbroom line-scanning HSI system (400–1000 nm) to detect chilling injury in white button mushrooms, with 98 % of freeze-damaged samples correctly classified.

With respect to internal defects, Ariana and Lu [6] developed a method for detecting internal quality of pickling cucumbers using simultaneous reflectance and transmittance hyperspectral imaging. They found that the transmittance mode detected the internal defect better compared to the reflectance mode. The simultaneous reflectance and transmittance combined the advantages of the two methods for internal defect detection. Average classification accuracy of 99 % was achieved.

The absorption of incident light, related to the chemical composition of a sample, allows quick answers to certain parameters in the evaluation of fruits and vegetables; for example, at wavelengths in the range of 670–710 nm, the absorption is higher in the presence of chlorophyll, a pigment that can be used as an indicator of maturity in different fruits such as bananas [98], apples [25] or peaches [63]. In vegetables at a wavelength of 675 nm, higher light absorption occurs by the presence of high concentrations of chlorophyll, for example in tomatoes in the green state (Fig. 3b). In ripe tomatoes, which contain more anthocyanins, greater light absorption occurs at a wavelength of 535 nm, which can be exploited by applying HSI to identify and select a sample of this vegetable when optimal maturity is evaluated [94].

Another aspect to consider in the quality of the fresh fruits and vegetables is the firmness. For example, firmness is related to scattering of incident light when the HSI is evaluated, showing greater light scattering in firm products, which Qin and Lu [94] related to the high content of pectin present in the structure of cell walls. In regard to tomatoes, the authors correlated firmness and ripeness using spectral data obtained by a hyperspectral system at wavelengths in the range of 500–1000 nm, with the maximum correlation coefficient $R = 0.66$, obtained at 790 nm.

The firmness also can be used as an indicator of maturity in different fruits such as bananas, apples or peaches. In this sense, hyperspectral imaging technique was used successfully to predict the quality attributes such as total soluble solids, moisture and firmness of the banana fruits, with coefficients of determination (R^2) of 0.85, 0.87 and 0.91, respectively, working at wavelengths of 400–1000 nm [98]. Moreover, Tallada et al. [111] conducted a NIR hyperspectral investigation for firmness prediction of strawberry at wavelengths of 650–1000, with a correlation of 0.79. Besides, it highlighted the importance of chlorophyll absorbance, around 680 nm, like was mentioned previously.

On the other hand, hyperspectral imaging was used by Noh and Lu [80] in the range of 500–1040 nm for the determination of firmness in apples with a correlation coefficient equal to or greater than 0.74. A similar study was done by Peng and Lu [86], who developed an optimal model for predicting quality attributes of apple fruit at wavelengths of 450–1000 nm, obtaining correlation coefficients of 0.89 and 0.88 for firmness and soluble solids, respectively. Similar results for firmness and soluble solids in apple ($R = 0.84$ and $R = 0.86$, respectively) were obtained by Qin et al. [95], working with hyperspectral scattering images, as shown in Table 2.

In another kind of fruit, Lu and Peng [63] utilized hyperspectral images (500–1000 nm) for the prediction of peach firmness and obtained the best prediction model at a wavelength of 677 nm (chlorophyll absorption), with values for R^2 of 0.77 and 0.58 for two different varieties of peach, respectively.

It is possible to determine the moisture content at different stages of fruit ripening. For example, while banana matures, the water content in the shell is declining, affecting the amount of reflected light at certain wavelengths; for example, the reflectance is less between 800

and 960 nm [98]. HSI has also been applied to assess the moisture content, total soluble solids and pH in strawberries in the spectral range of 400–1000 nm, with correlation coefficients (R) of 0.87, 0.80 and 0.92, respectively [24]. Thus, determining the moisture in fruit with HSI, it allows to take appropriate measures to prevent possible defects associated with high moisture content, a critical aspect in terms of stability during food preservation [2].

For its part, Zhao et al. [135] predicted sugar content in apples by hyperspectral imaging (685–900 nm) and obtained optimum spectral range of 704–805 nm for sugar content with $R = 0.91$. Liu et al. [59] measured the soluble solids of orange using a hyperspectral laser-induced fluorescence imaging technique (700–1100 nm). They gave good results with the correlation coefficient of 0.998 and 0.96 for two different varieties of orange, respectively. Besides, Menesatti et al. [69] successfully applied NIR hyperspectral imaging (1000–1700 nm) to evaluate starch index in apple, which is very crucial for maturity and harvest time determination. They obtained average classification accuracy of 80.8 %.

On the other hand, many fruits and vegetables, beside be consuming in fresh condition are destined for the production of other types of food and because of that they should present an ideal condition of maturity which is going to determine that the obtained product is a suitable quality product. For example in the development of red wine, grape must present adequate technological maturity, in addition to important parameters such as sugar content, acidity, pH and above the content of phenolic compounds [70]. In this regard, various studies have approached the study of the anthocyanin content in red grapes by applying HSI, which traditionally is done by physical and chemical methods that require investment of time and are of a destructive nature.

Nogales-Bueno et al. [77] developed a model to correlate spectral data with grape skin total phenolic concentration, sugar concentration, titratable acidity and pH in red and white grapes by modified partial least squares regression (MPLS) at wavelengths in the range of 950–1650 nm. The coefficients of determination (R^2) obtained for red grape samples for total phenolic concentration, °Brix for sugar concentration, titratable acidity and pH were 0.89, 0.99, 0.98 and 0.94, respectively. For white grape samples, the R^2 values were 0.80, 0.95, 0.93 and 0.94, respectively. Later, the same team [78] developed a model to correlate spectral data (900–1700 nm) with red grape skin extractable polyphenols. The obtained results (R^2) for the developed models were 0.82 for extractable total phenolic content, 0.79 for extractable anthocyanin content and 0.82 for extractable flavanol content. Also, they achieved the differentiation of four red grapes varieties (Garnacha, Graciano, Mazuelo and Tempranillo), for which 86, 52 and 86 % of the samples were correctly classified using anthocyanin profile, color image analysis and NIR hyperspectral imaging (950–1650 nm), respectively [79].

Similar studies were carried out to demonstrate the capability of hyperspectral imaging in predicting anthocyanin content changes in wine grapes during ripening. Chen et al. [12], working at wavelengths in the range of 900–1700 nm, obtained a $R^2 = 0.94$, highest value than $R^2 = 0.65$ obtained by Fernandes et al. [30].

Legumes, Cereals and Other Grains

Compared to other traditional techniques such as spectroscopy, the HSI has the advantage of conducting applications in individual grains, which is quite difficult to measure due to the heterogeneity of their structure [28]. Numerous applications have been achieved using this technology, as shown in Table 3, since the classification of grains and damage detection to analysis of certain constituents.

The hardness can be used to classify the grains, such as the work done by Williams et al. [120], who detected vitreous endosperm (hard) and floury (soft) in corn kernels using two hyperspectral imaging systems at wavelength in the range of 960–1662 and 1000–2498 nm, with coefficients of determination values of 0.85 and 0.76 %, respectively, similar to work developed by Manley et al. [68], who evaluated the texture of yellow maize endosperm, using a system HSI at wavelengths between 1000 and 2498 nm, with a $R^2 = 0.85$.

Traditionally, cereals assessment is performed based on the morphological characteristics of the core, such as size, shape, color and appearance. Moreover, the protein content is one of its most important characteristics, which has an effect on the functional properties of processed products, such as bread [66]. It has also evaluated the chemical composition of corn kernels [118] by acquiring reflectance images in a spectral range of 950–1700 nm, to predict concentrations derived from oleic acid in grains of corn, with R^2 of 0.68 and 0.65 for oil and oleic acid content, respectively. Similar studies were done on detection of oil content by NIR hyperspectral imaging in single maize kernels [18] at 750–1090 nm with $R^2 = 0.54$ and in sesame seeds [124] at wavelengths between 974 and 1734 nm with high classification accuracy (>96 % of classification rate).

Also, HSI technology was evaluated for predicting the moisture content in single kernels of maize [18], with a coefficient of determination $R^2 = 0.87$, and in soybean [41, 42], with a correlation coefficient $R = 0.97$, as shown in Table 3.

Besides, Mahesh et al. [64] investigated the feasibility of using the NIR hyperspectral imaging (960–1700 nm) for identifying different wheat classes. Classification accuracies were greater than 90 %. Later, Choudhary et al. [16]

Table 3 HSI applications in evaluating the quality and safety of cereals, legumes and other grains

Product	Application	λ (nm)	Accuracy	References
Wheat	Identification of classes	960–1700	>92 %	[16]
	Identification of classes	960–1700	>90 %	[64]
	Identification of classes at different moisture levels	960–1700	72–100 %	[65]
	Detection of insect damage	1000–1700	85–100 %	[104]
	Detection of midge damage	700–1000	95–99 %	[105]
	Detection of insect damage	700–1100	91–100 %	[106]
	Aspergillus niger	1000–1600	93 %	[133]
	Aspergillus glaucus	1000–1600	87 %	[133]
	Penicillium	1000–1600	99 %	[133]
	Detection of fusarium damage	400–1700	95 %	[21]
	Prediction of α-amylase activity	1000–2500	80 %	[126]
Corn	Moisture content	750–1090	$R^2 = 0.87$	[18]
	Oil content	750–1090	$R^2 = 0.54$	[18]
	Oil content	950–1700	$R^2 = 0.68$	[118]
	Oleic acid content	950–1700	$R^2 = 0.65$	[118]
	Classification based on the endosperm hardness	960–1662	$R^2 = 0.85$	[120]
	Classification based on the endosperm hardness	1000–2498	$R^2 = 0.76$	[120]
	Endosperm texture in maize kernels	1000–2498	$R^2 = 0.85$	[68]
	Fusarium infection	1000–2498	$R^2 = 0.98$	[119]
	Analysis of aflatoxin B1	400–2500	$R^2 = 0.80$	[31]
	Analysis of aflatoxin B1	400–1000	98 %	[115]
	Analysis of aflatoxin B1	1100–1700	97 %	[51]
Barley	Analysis of aflatoxin B1	400–2500	$R^2 = 0.85$	[31]
Rice	Growth of *Aspergillus oryzae*	400–1000	$R^2 = 0.97$	[107]
Soy	Color	400–1000	$R = 0.86$	[41]
	Moisture content	400–1000	$R = 0.97$	[42]
Sesame	Oil content	874–1734	>96 %	[124]

R correlation coefficient, R^2 coefficient of determination

identified wheat classes using bulk sample images taken from the NIR hyperspectral (960–1700 nm) with high average classification accuracies (>92 %).

The HSI has also been used to analyze the presence of external contaminants that may constitute a danger to the proper conservation of cereals and consumer. In this regard, Singh et al. [104] developed a method for sorting wheat grains, healthy and contaminated by insects, using NIR HSI to 1000–1700 nm, and high classification accuracy (85–100 %) in identifying healthy and insect-damaged kernels of wheat was obtained. Later, the same team [105] assessed the potentiality of shortwave NIR hyperspectral imaging (700–1000 nm). The highest classification accuracies were 95–99 % to discriminate healthy and midge-damaged wheat kernels. Other studies focused on the control of parasites in products such as soybeans and other legumes [11, 46].

In food safety, an application of the HSI is the detection of mycotoxins and aflatoxins produced by *Aspergillus flavus* and *Aspergillus parasiticus* that grow naturally in corn, peanuts and a wide variety of grains. The conventional method of determining aflatoxin requires ground grain and chemical analysis. Preliminary results revealed that the HSI technology has the potential to quantify the levels of aflatoxin contamination [81, 115]. It has been suggested that the presence or absence of the toxin can be determined from the HSI technique combined with UV radiation. This is because certain photosensitive components are excited to fluoresce in the visible and UV [131]. Fernández-Ibañez et al. [31], applying the HSI at wavelengths between 400 and 2500 nm, obtained coefficients of determination (R^2) of 0.80 and 0.85 for aflatoxin B1 in samples of corn and barley. Similar work was developed by Kandpal et al. [51] and Wang et al. [115] who reached high rates of classification of infected kernels (97 and 98 %, respectively), operating at wavelengths of 400–1000 and 1100–1700 nm, respectively.

In another investigation, Zhang et al. [133] evaluated the classification of wheat kernels infected by different fungal species using NIR hyperspectral images at a wavelength

region of 1000–1600 nm. Classification accuracies of 93, 87 and 99 % were achieved for identifying wheat kernels infected by *A. niger*, *A. glaucus* and *Penicillium* spp., respectively. Similar result (classification accuracy of 95 %) was obtained by Delwiche et al. [21] who detected fusarium damage in wheat at wavelength between 400 and 1700 nm.

In other cereals, Williams et al. [119] evaluated corn kernels infected with *Fusarium verticillioides*, applying NIR hyperspectral imaging (1000–2498 nm), with a coefficient of determination $R^2 = 0.98$. Besides, it highlighted two prominent peaks at 1900 and 2136 nm, related to changes in starch and protein compositions in the presence of *Fusarium*. Similar work was done by Siripatrawan and Makino [107], who developed a method for monitoring spoilage fungal growth on stored brown rice inoculated with *Aspergillus oryzae* using hyperspectral imaging at 400–1000 nm. HSI was able to rapidly identify infected rice, although the samples showed no symptoms of fungal infection, with a coefficient of determination $R^2 = 0.97$.

Meats

In today's markets, the demand for quality products and safety of the consumer is increasing. This is making the food industry to implement technologies that permit evaluation and quality control more quickly; control is done manually in many meat products, which is labor intensive, costly, slow and subject to human error.

Table 4 shows some research in the evaluation of the quality of meat, including tenderness analysis, microbial contamination, chemical composition.

A property with which a consumer qualifies meat is tenderness, a property manifested by a low resistance to breakdown in chewing. The opposite is the hardness, which is a textural property manifested by resistance, high and persistent breaking in chewing [45]. In cooked meats, texture involves two main components: tenderness and juiciness. With less juice, meat is considered less tender [22]; hence, it has become a challenge for the meat industry to measure this important parameter of quality effectively, accurately and noninvasively [73]. Techniques such as spectroscopy have shown a reasonable ability to predict meat tenderness [3]. Likewise, computer vision as a basis for predicting the characteristics of texture, marbled and color [43]. For its part, the HSI has proved to be a technique of wide applicability in this respect, since it simultaneously collects muscle structure and biochemical information that has a high degree of relationship with the softness of the flesh. Muscle structure and biochemical properties include muscle pH (that influences the activity of proteolytic enzymes), sarcomere length (an indication of the degree of muscle contraction in rigor), the degree of proteolysis, the amount and insolubility of tissue connective (collagen) and composition [29].

In several studies, the HSI has been applied to predicting the tenderness in the meat, based on indirect prediction of tenderness by extracting spectral data in some regions of the fillets and then interacting with actual values of tenderness determined by specialized instruments [28]. In this regard, Naganathan et al. [71, 72] used in the HSI spectral ranges of 400–1000 and 900–1700 nm to predict the tenderness of the cooked meat after 14 days of aging. The HSI obtained related to tenderness values obtained by shear force, predicting the different categories of meat samples depending on the tenderness in soft, medium and hard, with accuracy of 96.4 % [71]. Furthermore, wavelengths (1074, 1091, 1142, 1176, 1219, 1365, 1395, 1408 and 1462 nm) for the absorption of fat, protein and water were identified, although in this case the overall prediction accuracy of tenderness was only 77 % [72].

Other studies carried out to predict the tenderness in beef were developed by [73], at wavelength between 450 and 900 nm. The accuracy obtained was 93 %. Correlation coefficients of 0.67, 0.94 and 093, respectively, were obtained by Cluff et al. [17], Peng and Wu [87] and Tao et al. [112], working at similar spectral bands, as shown in Table 4.

Various studies were carried out to demonstrate the capability of hyperspectral imaging for identification and authentication of different red meat species. In this regard, Kamruzzaman et al. [48] achieved classification of beef, pork and lamb by images acquired at 900–1700 nm from *longissimus dorsi* muscle of these species. Classification accuracies of 99, 93 and 97 % were obtained. Also, the same work team [49] developed a nondestructive method for detecting adulteration in minced lamb meat, obtaining a coefficient of determination of 0.98.

Another parameter evaluated using HSI is the presence of tumors in poultry [52, 56], which are difficult to detect with the naked eye or by any technical traditional optics. In this regard, Kim et al. [52] developed a system of fluorescence HSI at wavelengths between 425 and 711 nm to detect tumors in the skin of chicken carcasses with a success rate of 76 %, but were not able to detect some tumors with a diameter of less than 3 mm. In other studies, at same wavelengths, best detection rates of tumors were obtained by Kong et al. [56] and Kim et al. [53], with values of 82 and 98 %, respectively. Also, the presence of bones in chicken fillets was evaluated by Yoon et al. [132], who obtained a 100 % of accuracy, applying HSI at 400–1000 nm.

Due to its richness in nutrients, meats are susceptible to microbial contamination, which can affect preservation and constitute a danger for the consumer. Currently, there is no technology to detect quickly and accurately bacterial

Table 4 Applications of HSI in assessing the quality and safety in meat and meat products

Product	Application	λ (nm)	Accuracy	References
Beef	Prediction of tenderness	496–1036	$R = 0.67$	[17]
	Prediction of tenderness	400–1000	96.4 %	[71]
	Prediction of tenderness	900–1700	77 %	[72]
	Prediction of tenderness	450–900	92.9 %	[73]
	Prediction of tenderness	400–1100	$R = 0.94$	[87]
	Identification and authentication	900–1700	99 %	[48]
	Determination of pigments	328–1115	$R^2 = 0.95$	[129]
	Total viable count of bacteria	400–1100	$R^2 = 0.96$	[89]
	Total viable count of bacteria	400–1000	$R^2 = 0.95$	[88]
Pork	Meat quality	400–1000	85 %	[90]
	Meat quality	430–980	87.5 %	[91]
	Identification and authentication	900–1700	93 %	[48]
	Recognition of freshness	900–1700	98 %	[8]
	Drip loss	430–980	$R = 0.77$	[92]
	pH of meat	430–980	$R = 0.55$	[92]
	Color of meat	430–980	$R = 0.86$	[92]
	pH in salted meat	400–1000	$R^2 = 0.79$	[60]
	Moisture content in salted pork	400–1000	$R^2 = 0.92$	[61]
	Total viable count	900–1700	$R^2 = 0.82$	[7]
	Psychrotrophic plate count	900–1700	$R^2 = 0.85$	[7]
	Prediction of tenderness	400–1100	$R = 0.93$	[112]
	E. coli contamination	400–1100	$R = 0.88$	[112]
Chicken meat	Detection of bone in fillets	400–1000	100 %	[132]
	Detection of skin tumors	425–711	76 %	[52]
	Detection of skin tumors	425–711	82 %	[56]
	Detection of skin tumors	425–711	98 %	[53]
	Detection of fecal contamination	400–1000	99 %	[40]
	Detection of fecal contamination	430–900	96 %	[84]
	Detection of fecal contamination	400–900	97 %	[83]
	Classification of fecal and ingesta contaminants	400–900	90 %	[85]
	Detection of diseases	400–900	93.5 %	[130]
	Difference between free-range and broiler chicken	328–1115	93 %	[127]
Lamb	Classification of muscle	900–1700	100 %	[47]
	Identification and authentication	900–1700	97 %	[48]
	Detection of adulteration	900–1700	$R^2 = 0.98$	[49]
Fish meat and marine products	Freshness of cod	892–2495	$R^2 = 0.59$	[10]
	Content of water	760–1040	$R = 0.94$	[27]
	Content of fat	760–1040	$R = 0.91$	[27]
	Oxidation of lipid	400–1000	$R^2 = 0.83$	[15]
	Total viable microorganisms in carp	400–1000	$R^2 = 0.90$	[14]
	Total viable microorganisms in salmon flesh	400–1700	$R^2 = 0.99$	[123]
	Freshness in frozen/unfrozen prawns	400–1000	95 %/98 %	[19]

R correlation coefficient, R^2 coefficient of determination

contamination; available methods are slow and destructive. In this regard, several studies have been conducted to assess impairment, as developed in porcine meat by Wang et al. [117], who explored the potential of HSI obtained by reflectance to predict the presence of total viable microorganisms achieving a high prediction ($R^2 = 0.94$).

Similar results were obtained in beef steaks, with coefficients of determination R^2 of 0.95 [88] and 0.96 [89], both working at 400–1000 nm, while in porcine meat, lower values of R^2 were obtained by Barbin et al. [7] for total viable count (TVC) and psychrotrophic plate count (PPC), with values of 0.82 and 0.85, respectively, at spectral region between 900 and 1700 nm. For its part, Tao et al. [112] obtained a correlation coefficient R of 0.88 in a nondestructive method for determination of *Escherichia coli* contamination in porcine meat, working with HSI of pork samples collected in the range of 400–1100 nm.

In fish meat, coefficients of determination R^2 of 0.90 for fresh grass carp [14] and 0.99 for salmon flesh [123] were obtained, as shown in Table 4.

Another form of contamination of the meat is through fecal matter, primarily in channels poultry. In this case, detection of contaminants basically depends on the spectral difference between contaminated skin and normal skin [83]. In this regard, Heitschmidt et al. [40] and Park et al. [83–85] have developed methods to detect fecal contamination in chicken meat using HSI at wavelengths between 400 and 1000 nm, in which the classification accuracies obtained were greater than 90 % in all cases, as shown in Table 4.

On the other hand, the quality of meats involves other parameters such as freshness, color, drip loss, water and fat contents, or pH. Regarding drip loss, pH and color of meat, Qiao et al. [92] investigated the potential of hyperspectral imaging (430–980 nm) for measuring these important parameters in porcine meat, getting correlation coefficients of 0.77, 0.55 and 0.86, respectively, while, in other work, Liu et al. [60] obtained in the same spectral band a coefficient of determination $R^2 = 0.79$ for pH in salted meat of pork.

With respect to the freshness, various studies were carried out in different classes of meat. For example, Barbin et al. [8] achieved a correct classification of 98 % for discrimination between fresh and frozen-thawed pork based on reflectance in the NIR wavelength range of 900–1700 nm.

Besides, freshness is recognized as a main element of fish quality. The direct key functions of storage time and temperature have a significant influence on fish freshness. Chau et al. [10] evaluated the freshness of codfish, based on color changes of the eyes, fillets and gill filaments, as a function of days on ice, by HSI at wavelength of 900–2500 nm, information that correlated with color parameters obtained by CIELAB system, getting a coefficient of determination of 0.59. An increase in the lightness as the color of the eyes changed rapidly from black to cloudy white during the period of storage was observed. Besides, as might be expected, the main color change in fillets during storage was an increase in yellowness, while gill filaments showed a typical characteristic change from a deep red color to a pale yellow color with time. In a recent study, Dai et al. [19] investigated the potential of visible and NIR hyperspectral imaging (400–1000 nm) as a rapid and noninvasive method to differentiate freshness of prawns. The results demonstrated a satisfactory classification rate of 98 and 95 % for prediction samples in unfrozen and frozen groups, respectively.

Another application in meat of the HSI is the characterization and distribution of different chemical attributes. For a detailed analysis of food, the concentration gradients of certain chemical components are more easily measured than the average concentrations due to the heterogeneity of the sample, as in the case of meat and meat products. In this regard, the HSI constitutes a great potential to determine the chemical composition in meat products as demonstrated in previous studies [27, 82].

It is known that fat and water concentrations vary in different parts of the fillet, so that a system that provides the exact chemical composition and spatial distribution that allows real-time online monitoring, is a necessity. This would ensure proper classification and control manufacturing processes, such as controlling the fat and salt content in the salted and smoked salmon, as shown by previous studies, in which good prediction levels were obtained, with a correlation coefficient $R = 0.97$ and a prediction error of 1.95 %, for fat content [100], and $R = 0.86$ and a prediction error of 0.56 %, for NaCl content [101], using near-infrared (NIR) interactance imaging. For its part, Liu et al. [61] used HSI (400–1000 nm) for predicting the moisture content of porcine meat during salting process, obtaining a $R^2 = 0.92$.

In fish fillets, the water and fat contents also have been measured [27], using a nondestructive method of spectral imaging (760–1040 nm). The correlation coefficients obtained for water content and fat content were 0.94 and 0.91, respectively.

Similarly, it is possible to determine the content of intramuscular fat in pork using the HSI in a spectral range of 1193–1217 nm [41, 42]. The intramuscular fat content affects the quality of pork, affecting the flavor and juiciness, and even health, determinants of consumer satisfaction. Therefore, different levels of fat content may result in different levels of acceptance.

After slaughter, the pH is one of the most important parameters to evaluate meat [60], which has an influence on the texture, water-holding capacity, resistance to microbial growth and color [34, 37]. So, setting a pH level of about 5.5 is very important to inhibit certain critical enzymes (such as phosphofructokinase) and cease metabolic reactions (such as glycolysis) [103]. Anaerobic glycolysis postmortem is the metabolic pathway that occurs in the muscle of the slaughtered animal, leading to the formation of lactic acid and a decrease in pH.

The relationship between the chemical composition and texture and other sensory attributes of the meat is not limited to the presence of fat or pH, but also includes the occurrence of other compounds, such as collagen. Hydroxyproline, collagen constituent amino acid, was also analyzed using HSI at wavelengths between 400 and 1000 nm [128].

HSI has been used for the detection of parasites in fish fillets, which are regarded as a quality problem in the fishing industry. The traditional way to detect them is by manual examination. The HSI has proven to be an effective technique for automatic detection of parasites and blood stains on fish fillets, by the difference between the spectral patterns of these defects and healthy meat [28]. With HSI, it is also possible to determine the spatial distribution of these parasites in the fish meat, which facilitates the process of removing these defective sections [39].

One of the pioneering studies in this regard was that developed by Wold et al. [121], to assess cod fillets using multispectral imaging at wavelengths between 400 and 1000 nm, detecting parasites inside the fillets up to 6 mm deep. Greater depth of detection, 8 mm, was subsequently achieved by applying hyperspectral images at wavelengths of 350–950 nm [39]. This shows the great advantage of the HSI compared with multispectral imaging, since it can detect parasites in greater depth, and obviously greater depth than is usually achieved by visual inspection, widely used in the industry.

The meat stored can be hazardous to the consumer. With HSI, it is possible to assess the deterioration of meat at different storage conditions. In this regard, Cheng et al. [15] evaluated lipid oxidation in fillets carp (*Ctenopharyngodon idella*) using HSI to determine the value of thiobarbituric acid (TBA) at wavelengths of 400–1000 nm with a $R^2 = 0.83$. Increasing TBA is caused by the formation of secondary products resulting from lipid oxidation, such as *n*-alkanes, especially the malonaldehyde [113], considered carcinogenic substance.

Dairy and Egg Products

Traditional technologies such as spectroscopy were used to characterize quality parameters and composition in dairy products [28]. Unlike other food groups, studies conducted with application of HSI in dairy products are rare; however, Table 5 shows some examples.

In dairy products, it is possible to measure the chemical composition based on the spectral information of each constituent, which can, for example, classify cheeses based on their fat content (half and full fat) [36], using an HSI system spectral range 400–1000 nm, for comparison with RGB images of the cheese samples studied (obtained using a digital camera). The results indicated that images acquired from the full-fat products reflect more light in the visible (500–950 nm) wavelength range. These spectral features may be used to classify each pixel of the HSI into one of two or more groups. Qin and Lu [93] used a HSI system for measuring the absorption and scattering properties of turbid food materials over the visible and NIR region of 530–900 nm. Values of the absorption and reduced scattering coefficient at 600 nm were highly correlated to the fat content of the milk samples, with correlation coefficients of 0.995 and 0.998, respectively.

In another work, Burger and Geladi [9] predicted the composition of commercial cheeses, using an HSI system at wavelengths between 960 and 1662 nm, based on the specific spectral information of each constituent. Root-mean-square error of prediction (RMSEP) was used as a general indicator to predict the cheese constituents, getting RMSEP values of 1.8, 0.7 and 1.3, respectively, for proteins, fats and carbohydrates contents.

Table 5 Applications of HSI in evaluation of dairy and egg products

Product	Application	λ (nm)	Accuracy	References
Cheese	Prediction of protein	960–1662	RMSEP = 1.8	[9]
	Prediction of fat	960–1662	RMSEP = 0.7	[9]
	Prediction of carbohydrates	960–1662	RMSEP = 1.3	[9]
Milk	Content of fat	530–900	$R = 0.995$	[93]
	Detection of melamine adulteration in milk powder	990–1700	<200 ppm	[32]
Eggs	Content of omega-3 fatty acids:			
	α-Linolenic	900–1700	$R = 0.94$	[1]
	EPA	900–1700	$R = 0.73$	[1]
	DHA	900–1700	$R = 0.87$	[1]
	Freshness	380–1010	$R^2 = 0.87$	[134]
	Internal bubbles	380–1010	90 %	[134]
	Scattered yolk	380–1010	96 %	[134]

R correlation coefficient, R^2 coefficient of determination, *RMSEP* root-mean-square error of prediction, *EPA* eicosapentaenoic acid, *DHA* docosahexaenoic acid

HSI was also used to evaluate the presence of external agents which may present a danger to the preservation of the product and the consumer, for example waste plastic products remaining after the production process. In this regard, Gowen et al. [36] detected plastic remains (3 mm of plastic) based on the spectral pattern of cheese samples at a range of 950–1650 nm. The plastic contaminant exhibited a sharp absorption band at around 1170 nm.

Also, detection of adulteration in milk was studied by Fu et al. [32], who achieved detection of melamine adulteration in milk powders at very low concentrations (<200 ppm) using NIR hyperspectral imaging at wavelength in the range of 990–1700 nm, and the most significant spectral difference between melamine and milk was observed at around 1473.8 nm, which is due to the aromatic amine structures. Melamine was recently found to have been deliberately added to milk formula and animal feed to increase the apparent protein content of the products, causing illnesses and deaths for a significant number of infants [97].

In regard to eggs, important parameters related to internal quality were evaluated by Zhang et al. [134], who developed a nondestructive test based on hyperspectral imaging (380–1010 nm), to determine the internal quality of eggs, including freshness, bubble formation or scattered yolk. For freshness, they achieved a coefficient of determination $R^2 = 0.87$, while eggs with internal bubbles and scattered yolk could be discriminated with identification accuracy of 90 and 96 %, respectively.

Another important aspect in the modern food industry is the design of food, the consumption of which not only provides the nutrients the body needs, but also provides other benefits that help maintain optimal health, such as functional foods. In this sense, the HSI can also be applied to characterize these types of foods, such as to assess the content of certain molecules that give character to the functional food. In this regard, the content of omega-3 eggs was evaluated at wavelengths between 900 and 1700 nm [1], which achieved correlation coefficients of 0.94, 0.73 and 0.87, respectively, for α-linolenic, eicosapentaenoic and docosahexaenoic acids.

This study would classify products for their high content of omega-3 to be marketed as functional foods to a higher sales price, achieving greater economic benefits. This could also be applied to other foods with significant omega-3 levels, such as olive oil, flaxseed, some nuts, or also applied to other molecules that give certain foods a functional nature, such as anthocyanins, dietary fiber, vitamins, phytosterols.

Current and Future Challenges

HSI applications in food are showing a positive trend, especially since 2011 (Fig. 1), and focusing more and more on new types of food. In terms of food groups, the preference has always been on the fruit, then the meat and then vegetables. It is important to note that since 2010, dairy products have begun to appear with a large proportion of published research (Fig. 1), perhaps because it is now important to study the application of HSI on products that are mostly consumed by society.

This could be happening in response to a demand for technology of the following characteristics: (a) reliable and accurate, (b) adaptable to different processes, (c) rapid retrieval of information, and (d) cheaper. As a new technology, the HSI still faces challenges to its full exploitation, such as difficulty in handling large amounts of data, low-speed and high-cost calculation, aspects that must be addressed in future research in order to optimize its application in food industry.

Current studies are aiming at identifying optimal wavelengths for each food or food constituents, so they can design systems to obtain real-time information necessary to facilitate better decision-making regarding product features to develop, which must comply with quality and safety requirements established. Similarly, given the large amount of data from the wide range of spectral bands in which the HSI works, continue developing new models that allow rapid discrimination data and get only information of interest. In the immediate future, it is expected that these problems can be overcome, as well as related to the high cost of implementing the HSI in the different processes in the food industry, so that it is possible to access this technology and maximize its benefits.

Thus, it is expected that the use of this technology to evaluate the quality and safety of food becomes necessary for industry. All these could result in improvements of the products in real time, without having to stop the processes that require high costs to industry.

Conclusions

In the modern food industry, the requirement for adequate control of attributes such as size, shape, color and texture of foods is greater. This requirement is fulfilled by automated or by visual inspection techniques, which often can lead to human error. Furthermore, evaluation of parameters related to the food composition such as moisture content, fat, protein often requires destructive analysis that demands the use of both human and technological resources that make them unworkable in practice.

These parameters can be measured simultaneously by the HSI, which allows to obtain data on a larger number of spectral bands, making them a better source of information for assessing the external attributes and predicting the composition and spatial distribution of the various constituents within the food, besides providing speed,

reliability, accuracy, reduced human error in the analysis and not be destructive.

HSI offers the advantage of evaluating samples of heterogeneous nature, by other techniques, such as simple spectroscopy, which would be limited only to the characterization of homogeneous materials, which is inefficient in a practical application that must control the entire surface of a sample.

Finally, despite presenting some disadvantages such as long time that is required for data acquisition and processing of this information, it is anticipated that the use of this technology will become indispensable in the industry, to evaluate the quality and safety of food, providing that improvements are made in terms of real-time control and safety control requirements.

Acknowledgments Raúl Siche thanks the following institutions for funding: Fondo para la Innovación, la Ciencia y la Tecnología—FINCyT (Contract 407-PNICP-PIAP-2014) and Universidad Nacional de Trujillo—UNT (PIC2-2013/UNT). Erick Saldaña thanks the "Ministerio de Educación del Perú" for the scholarship granted by the program "Programa Nacional de Becas y Crédito Educativo" (PRONABEC).

References

1. Abdel-Nour N, Ngadi M (2011) Detection of omega-3 fatty acid in designer eggs using hyperspectral imaging. Int J Food Sci Nutr 62(4):418–422
2. Achata E, Esquerre C, O'Donnell C, Gowen A (2015) A study on the application of near infrared hyperspectral chemical imaging for monitoring moisture content and water activity in low moisture systems. Molecules 20:2611–2621
3. Andrés S, Silva A, Soares-Pereira AL, Martins C, Bruno-Soares AM, Murray I (2008) The use of visible and near infrared reflectance spectroscopy to predict beef M. Longissimus thoracis et lumborum quality attributes. Meat Sci 78:217–224
4. Ariana DP, Lu R, Guyer DE (2006) Near-infrared hyperspectral reflectance imaging for detection of bruises on pickling cucumbers. Comput Electron Agric 53:60–70
5. Ariana DP, Lu R (2008) Quality evaluation of pickling cucumbers using hyperspectral reflectance and transmittance imaging: Part II. Performance of a prototype. Sens Instrum Food Qual Saf 2:152–160
6. Ariana DP, Lu R (2008) Detection of internal defect in pickling cucumbers using hyperspectral transmittance imaging. Trans ASABE 51:705–713
7. Barbin D, ElMasry G, Sun D-W, Allen P, Noha M (2012) Non-destructive assessment of microbial contamination in porcine meat using NIR hyperspectral imaging. Innov Food Sci Emerg Techol 17:180–191
8. Barbin D, Sun D-W, Su C (2013) NIR hyperspectral imaging as non-destructive evaluation tool for the recognition of fresh and frozen–thawed porcine *longissimus dorsi* muscles. Innov Food Sci Emerg Techol 18:226–236
9. Burger J, Geladi P (2006) Hyperspectral NIR image regression part II: dataset preprocessing diagnostics. J Chemom 20:106–119
10. Chau A, Whitworth M, Leadley C, Millar S (2009) Innovative sensors to rapidly and non-destructively determine fish freshness. Seafish Industry Authority Report No CMS/REP/110284/1
11. Chelladurai V, Karuppiah K, Jayas DS, Fields PG, White NDG (2014) Detection of *Callosobruchus maculatus* (F.) infestation in soybean using soft X-ray and NIR hyperspectral imaging techniques. J Stored Prod Res 57:43–48
12. Chen S, Zhang F, Ning J, Liu X, Zhang Z, Yang S (2015) Predicting the anthocyanin content of wine grapes by NIR hyperspectral imaging. Food Chem 172:788–793
13. Cheng X, Chen YR, Tao Y, Wang CY, Kim MS, Lefcourt AM (2004) A novel integrated PCA and FLD method on hyperspectral image feature extraction for cucumber chilling damage inspection. Trans ASAE 47(4):1313–1320
14. Cheng J-H, Sun D-W (2015) Rapid and non-invasive detection of fish microbial spoilage by visible and near infrared hyperspectral imaging and multivariate analysis. LWT Food Sci Technol 62(2):1060–1068
15. Cheng J-H, Sun D-W, Pu H-B, Wang Q-J, Chen Y-N (2015) Suitability of hyperspectral imaging for rapid evaluation of thiobarbituric acid (TBA) value in grass carp (*Ctenopharyngodon idella*) fillet. Food Chem 171:258–265
16. Choudhary R, Mahesh S, Paliwal J, Jayas DS (2009) Identification of wheat classes using wavelet features from near infrared hyperspectral images of bulk samples. Biosyst Eng 102:115–127
17. Cluff K, Naganathan GK, Subbiah J, Lu R, Calkins CR, Samal A (2008) Optical scattering in beef steak to predict tenderness using hyperspectral imaging in the VIS-NIR region. Sens Instrum Food Qual Saf 2:189–196
18. Cogdill RP, Hurburgh CR Jr, Rippke GR (2004) Single-kernel maize analysis by near-infrared hyperspectral imaging. Trans ASAE 47(1):311–320
19. Dai Q, Cheng J-H, Sun D-W (2015) Potential of visible/near-infrared hyperspectral imaging for rapid detection of freshness in unfrozen and frozen prawns. J Food Eng 149:97–104
20. Del Fiore A, Reverberi M, Ricelli A, Pinzari F, Serranti S, Fabbri AA, Bonifazi G, Fanelli C (2010) Early detection of toxigenic fungi on maize by hyperspectral imaging analysis. Int J Food Microbiol 144:64–71
21. Delwiche SR, Kim MS, Dong Y (2011) Fusarium damage assessment in wheat kernels by Vis/NIR hyperspectral imaging. Sens Instrum Food Qual Saf 5(2):63–71
22. Dransfield E (1999) In: Pearson AM, Dutson TR (eds) Quality attributes and their measurement in meat, poultry and fish products, vol 11. Aspen Publication, Maryland, pp 289–315
23. Du CJ, Sun DW (2004) Recent developments in the applications of image processing techniques for food quality evaluation. Trends Food Sci Technol 15:230–249
24. ElMasry G, Wang N, ElSayed A, Ngadi M (2007) Hyperspectral imaging for non-destructive determination of some quality attributes for strawberry. J Food Eng 81:98–107
25. ElMasry G, Wang N, Vigneault C, Qiao J, ElSayed A (2008) Early detection of apple bruises on different background colors using hyperspectral imaging. LWT Food Sci Technol 41:337–345
26. ElMasry G, Wang N, Vigneault C (2009) Detecting chilling injury in Red Delicious apple using hyperspectral imaging and neural networks. Postharvest Biol Technol 52(1):1–8
27. ElMasry G, Wold JP (2008) High-speed assessment of fat and water content distribution in fish fillets using online imaging spectroscopy. J Agric Food Chem 56(17):7672–7677
28. ElMasry G, Kamruzzaman M, Sun D-W, Allen P (2012) Principles and applications of hyperspectral imaging in quality evaluation of agro-food products: a review. Crit Rev Food Sci 52(11):999–1023
29. Felter LM (2007) Predicting aged beef tenderness with hyperspectral imaging and the relationship to muscle properties. Master's thesis: Animal Science. University of Nebraska-Lincoln, USA

30. Fernandes AM, Oliveira P, Moura JP, Oliveira AA, Falco V, Correia MJ, Melo-Pinto P (2011) Determination of anthocyanin concentration in whole grape skins using hyperspectral imaging and adaptive boosting neural networks. J Food Eng 105:216–226
31. Fernández-Ibañez V, Soldado A, Martínez-Fernández A, de la Roza-Delgado B (2009) Application of near infrared spectroscopy for rapid detection of aflatoxin B1 in maize and barley as analytical quality assessment. Food Chem 113:629–634
32. Fu X, Kim M, Chao K, Qin J, Lim J, Lee H, Garrido-Varo A, Pérez-Marín D, Ying Y (2014) Detection of melamine in milk powders based on NIR hyperspectral imaging and spectral similarity analyses. J Food Eng 124:97–104
33. Goetz AFH, Vane G, Solomon JE, Rock BN (1985) Imaging spectroscopy for earth remote sensing. Science 228:1147–1153
34. Gou P, Comaposada J, Arnau J (2002) Meat pH and meat fibre direction effects on moisture diffusivity in salted ham muscles dried at 5 °C. Meat Sci 61:25–31
35. Gowen AA, Taghizadeh M, O'Donnell CP (2009) Identification of mushrooms subjected to freeze damage using hyperspectral imaging. J Food Eng 93(1):7–12
36. Gowen AA, Burger J, O'Callaghan D, O'Donnell CP (2009b) Potential applications of hyperspectral imaging for quality control in dairy foods. In: 1st international workshop on computer image analysis in agriculture, Potsdam, Germany
37. Guerrero L, Gou P, Arnau J (1999) The influence of meat pH on mechanical and sensory textural properties of dry-cured ham. Meat Sci 52:267–273
38. Harvey AR, Lawlor J, McNaught AI, Fletcher-Holmes DW (2002) Hyperspectral imaging for the detection of retinal disease. Proc SPIE 4816:325–335
39. Heia K, Sivertsen AH, Stormo SK, Elvevoll E, Wold JP, Nilsen H (2007) Detection of nematodes in cod (*Gadus morhua*) fillets by imaging spectroscopy. J Food Sci 72(1):11–15
40. Heitschmidt GW, Park B, Lawrence KC, Windham WR, Smith DP (2007) Improved hyperspectral imaging system for fecal detection on poultry carcasses. Trans ASABE 50(4):1427–1432
41. Huang H, Liu L, Ngadi MO, Gariépy C (2014) Rapid and non-invasive quantification of intramuscular fat content of intact pork cuts. Talanta 119:385–395
42. Huang M, Wang Q, Zhang M, Zhu Q (2014) Prediction of color and moisture content for vegetable soybean during drying using hyperspectral imaging technology. J Food Eng 128:24–30
43. Jackman P, Sun D-W, Allen P (2010) Prediction of beef palatability from color, marbling and surface texture features of longissimus dorsi. J Food Eng 96(1):151–165
44. Jones HG, Vaughan RA (2010) Remote sensing of vegetation: principles, techniques and applications. Oxford University Press, New York
45. Jowitt R (1974) The terminology of food texture. J Texture Stud 5:351–358
46. Kaliramesh S, Chelladurai V, Jayas DS, Alagusundaram K, White NDG, Fields PG (2013) Detection of infestation by *Callosobruchus maculatus* in mung bean using near-infrared hyperspectral imaging. J Stored Prod Res 52:107–111
47. Kamruzzaman M, ElMasry G, Sun D-W, Allen P (2011) Application of NIR hyperspectral imaging for discrimination of lamb muscles. J Food Eng 104:332–340
48. Kamruzzaman M, Barbin D, ElMasry G, Sun D-W, Allen P (2012) Potential of hyperspectral imaging and pattern recognition for categorization and authentication of red meat. Innov Food Sci Emerg Techol 16:316–325
49. Kamruzzaman M, Sun D-W, ElMasry G, Allen P (2013) Fast detection and visualization of minced lamb meat adulteration using NIR hyperspectral imaging and multivariate image analysis. Talanta 103:130–136
50. Kamruzzaman M, Makino Y, Oshita S (2015) Non-invasive analytical technology for the detection of contamination, adulteration, and authenticity of meat, poultry, and fish: a review. Anal Chim Acta 853:19–29
51. Kandpal LM, Lee S, Kim M, Bae H, Cho B-K (2015) Short wave infrared (SWIR) hyperspectral imaging technique for examination of aflatoxin B_1 (AFB_1) on corn kernels. Food Control 51:171–176
52. Kim I, Kim MS, Chen YR, Kong SG (2004) Detection of skin tumors on chicken carcasses using hyperspectral fluorescence imaging. Trans ASAE 47(5):1785–1792
53. Kim I, Xu C, Kim MS (2006) Poultry skin tumor detection in hyperspectral images using radial basis probabilistic neural network. Adv Neural Netw 3973:770–776
54. Kim MS, Chen YR, Cho BK, Chao K, Yang CC, Lefcourt AM, Chan D (2007) Hyperspectral reflectance and fluorescence line-scan imaging for online defects and fecal contamination inspection of apples. Sens Instrum Food Qual Saf 1:151–159
55. Kim MS, Lefcourt AM, Chen Y, Tao Y (2005) Automated detection of fecal contamination of apples based on multispectral fluorescence image fusion. J Food Eng 71(1):85–91
56. Kong SG, Chen YR, Kim I, Kim MS (2004) Analysis of hyperspectral fluorescence images for poultry skin tumor inspection. Appl Opt 43(4):824–833
57. Lee H, Kim MS, Jeong D, Delwiche SR, Chao K, Cho B-K (2014) Detection of cracks on tomatoes using a hyperspectral near-infrared reflectance imaging system. Sensors 14:18837–18850
58. Liu Y, Chen YR, Wang CY, Chan DE, Kim MS (2005) Development of a simple algorithm for the detection of chilling injury in cucumbers from visible/near-infrared hyperspectral imaging. Appl Spectrosc 59(1):78–85
59. Liu M, Zhang L, Guo E (2008) Hyperspectral laser-induced fluorescence imaging for non-destructive assessing soluble solids content of orange. Comput Comput Technol Agric 1:51–59
60. Liu D, Pu H, Sun D-W, Wang L, Zeng X-A (2014) Combination of spectra and texture data of hyperspectral imaging for prediction of pH in salted meat. Food Chem 160:330–337
61. Liu D, Sun D-W, Qu J, Zeng X-A, Pu H, Ma J (2014) Feasibility of using hyperspectral imaging to predict moisture content of porcine meat during salting process. Food Chem 152:197–204
62. Lu R (2003) Detection of bruises on apple using near-infrared hyperspectral imaging. Trans ASAE 46(2):523–530
63. Lu R, Peng Y (2006) Hyperspectral scattering for assessing peach fruit firmness. Biosyst Eng 93(2):161–171
64. Mahesh S, Manickavasagan A, Jayas DS, Paliwal J, Whiteb NDG (2008) Feasibility of near-infrared hyperspectral imaging to differentiate Canadian wheat classes. Biosyst Eng 101:50–57
65. Mahesh S, Jayas DS, Paliwal J, White NDG (2011) Identification of wheat classes at different moisture levels using near-infrared hyperspectral images of bulk samples. Sens Instrum Food Qual Saf 5(1):1–9
66. Mahesh S, Jayas DS, Paliwal J, White NDG (2015) Hyperspectral imaging to classify and monitor quality of agricultural materials. J Stored Prod Res 61:17–26
67. Mahmoud B, Bachman G, Linton R (2010) Inactivation of *Escherichia coli* O157: H7, *Listeria monocytogenes*, *Salmonella enterica* and *Shigella flexneri* on spinach leaves by X-ray. Food Microbiol 27(1):24–28
68. Manley M, Williams P, Nilsson D, Geladi P (2009) Near infrared hyperspectral imaging for the evaluation of endosperm texture in whole yellow maize (*Zea maize* L.) kernels. J Agric Food Chem 57:8761–8769
69. Menesatti P, Zanella AS, D'Andrea S, Costa C, Paglia G, Pallottino F (2009) Supervised multivariate analysis of hyper-

spectral NIR images to evaluate the starch index of apples. Food Bioprocess Technol 2:308–314
70. Morata A, Loira I, Vejarano R, Bañuelos MA, Sanz P, Otero L, Suárez-Lepe JA (2015) Grape processing by high hydrostatic pressure: effect on microbial populations, phenol extraction and wine quality. Food Bioprocess Technol 8(2):277–286
71. Naganathan GK, Grimes LM, Subbiah J, Calkins CR, Samal A, Meyer GE (2008) Visible/near-infrared hyperspectral imaging for beef tenderness prediction. Comput Electron Agric 64:225–233
72. Naganathan GK, Grimes LM, Subbiah J, Calkins CR, Samal A, Meyer GE (2008) Partial least squares analysis of near-infrared hyperspectral images for beef tenderness prediction. Sens Instrum Food Qual Saf 2:178–188
73. Naganathan GK, Cluff K, Samal A, Calkins CR, Jones DD, Lorenzen CL, Subbiah J (2015) A prototype on-line AOTF hyperspectral image acquisition system for tenderness assessment of beef carcasses. J Food Eng 154:1–9
74. Nagata M, Tallada JG, Kobayashi T (2006) Bruise detection using NIR hyperspectral imaging for strawberry (*Fragaria x ananassa* Duch.). Environ Control Biol 44(2):133–142
75. Nguyen Do Trong NN, Tsuta M, Nicolaï BM, Baerdemaeker JD, Saeys W (2011) Prediction of optimal cooking time for boiled potatoes by hyperspectral imaging. J Food Eng 105(4):617–624
76. Nicolaï BM, Beullens EB, Peirs A, Saeys W, Theron KI, Lammertyna J (2007) Nondestructive measurement of fruit and vegetable quality by means of NIR spectroscopy: a review. Postharvest Biol Technol 46(2):99–118
77. Nogales-Bueno J, Hernández-Hierro JM, Rodríguez-Pulido FJ, Heredia FJ (2014) Determination of technological maturity of grapes and total phenolic compounds of grape skins in red and white cultivars during ripening by near infrared hyperspectral image: a preliminary approach. Food Chem 152:586–591
78. Nogales-Bueno J, Baca-Bocanegra B, Rodríguez-Pulido FJ, Heredia FJ, Hernández-Hierro JM (2015) Use of near infrared hyperspectral tools for the screening of extractable polyphenols in red grape skins. Food Chem 172:559–564
79. Nogales-Bueno J, Rodríguez-Pulido FJ, Heredia FJ, Hernández-Hierro JM (2015) Comparative study on the use of anthocyanin profile, color image analysis and near-infrared hyperspectral imaging as tools to discriminate between four autochthonous red grape cultivars from La Rioja (Spain). Talanta 131:412–416
80. Noh HK, Lu R (2007) Hyperspectral laser-induced fluorescence imaging for assessing apple fruit quality. Postharvest Biol Technol 43:193–201
81. Ononye AE, Yao H, Hruska Z, Kincaid R, Brown RL, Cleveland TE (2009) Automatic detection of aflatoxin contaminated corn kernels using dual-band imagery. Proc SPIE 7315:73150R
82. Ottestad S, Høy M, Stevik A, Wold JP (2009) Prediction of ice fraction and fat content in super-chilled salmon by non-contact interactance near infrared imaging. J Near Infrared Spectrosc 17(2):77–87
83. Park B, Lawrence KC, Windham WR, Buhr RJ (2002) Hyperspectral Imaging for detecting fecal and ingesta contaminants on poultry carcasses. Trans ASAE 45(6):2017–2026
84. Park B, Lawrence KC, Windham WR, Smith DP (2006) Performance of hyperspectral imaging system for poultry surface fecal contaminant detection. J Food Eng 75:340–348
85. Park B, Windham WR, Lawrence KC, Smith DP (2007) Contaminant classification of poultry hyperspectral imagery using spectral angle mapper algorithm. Biosyst Eng 96(3):323–333
86. Peng Y, Lu R (2008) Analysis of spatially resolved hyperspectral scattering images for assessing apple fruit firmness and soluble solids content. Postharvest Biol Technol 48:52–62
87. Peng Y, Wu J (2008) Hyperspectral scattering profiles for prediction of beef tenderness. American Society of Agricultural and Biological Engineers, St. Joseph, Michigan
88. Peng Y, Zhang J, Wang W, Li Y, Wu J, Huang H, Gao X, Jiang W (2011) Potential prediction of the microbial spoilage of beef using spatially resolved hyperspectral scattering profiles. J Food Eng 102:163–169
89. Peng Y, Zhang J, Wu J, Hang H (2009) Hyperspectral scattering profiles for prediction of the microbial spoilage of beef. Proc SPIE 7315:73150Q1–73150Q12
90. Qiao J, Ngadi MO, Wang N, Gariepy C, Prasher SO (2007) Pork quality and marbling level assessment using a hyperspectral imaging system. J Food Eng 83(1):10–16
91. Qiao J, Ngadi MO, Wang N, Gunenc A, Monroy M, Gariepy C, Prasher S (2007) Pork quality classification using a hyperspectral imaging system and neural network. Int J Food Eng 3(1):1–12
92. Qiao J, Wang N, Ngadi M, Gunenc A, Monroy M, Gariepy C, Prasher S (2007) Prediction of drip-loss, pH and color for pork using a hyperspectral imaging technique. Meat Sci 76(1):1–8
93. Qin J, Lu R (2007) Measurement of the absorption and scattering properties of turbid liquid foods using hyperspectral imaging. Appl Spectrosc 61(4):388–396
94. Qin J, Lu R (2008) Measurement of the optical properties of fruits and vegetables using spatially resolved hyperspectral diffuse reflectance imaging technique. Postharvest Biol Technol 49:355–365
95. Qin J, Lu R, Peng Y (2009) Prediction of apple internal quality using spectral absorption and scattering properties. Trans ASABE 52(2):499–507
96. Qin J, Chao K, Kim M, Lu R, Burks T (2013) Hyperspectral and multispectral imaging for evaluating food safety and quality. J Food Eng 118:157–171
97. Qin J, Chao K, Kim M (2010) Raman chemical imaging system for food safety and quality inspection. Trans ASABE 53(6):1873–1882
98. Rajkumar P, Wang N, Eimasry G, Raghavan GSV, Gariepy Y (2012) Studies on banana fruit quality and maturity stages using hyperspectral imaging. J Food Eng 108:194–200
99. Saldaña E, Siche R, Luján M, Quevedo R (2013) Review: computer vision applied to the inspection and quality control of fruits and vegetables. Braz J Food Technol 16(4):254–272
100. Segtnan VH, Høy M, Lundby F, Narum B, Wold JP (2009) Fat distributional analysis in salmon fillets using non-contact near infrared interactance imaging: a sampling and calibration strategy. J Near Infrared Spectrosc 17(5):247–253
101. Segtnan VH, Høy M, Sørheim O, Kohler A, Lundby F, Wold JP, Ofstad R (2009) Noncontact salt and fat distributional analysis in salted and smoked salmon fillets using X-ray computed tomography and NIR interactance imaging. J Agric Food Chem 57:1705–1710
102. Shaw G, Manolakis D (2002) Signal processing for hyperspectral image exploitation. IEEE Signal Process Mag 19(1):12–16
103. Shen QW, Means WJ, Underwood KR, Thompson SA, Zhu MJ, McCormick RJ, Ford SP, Ellis M, Du M (2006) Early post-mortem AMP-activated protein kinase (AMPK) activation leads to phosphofructokinase-2 and -1 (PFK-2 and PFK-1) phosphorylation and the development of pale, soft, and exudative (PSE) conditions in porcine longissimus muscle. J Agric Food Chem 54(15):5583–5589
104. Singh CB, Jayas DS, Paliwal J, White NDG (2009) Detection of insect-damaged wheat kernels using near-infrared hyperspectral imaging. J Stored Prod Res 45:151–158
105. Singh CB, Jayas DS, Paliwal J, White NDG (2010) Detection of midge-damaged wheat kernels using short-wave near-infrared hyperspectral and digital color imaging. Biosyst Eng 105:380–387
106. Singh CB, Jayas DS, Paliwal J, White NDG (2010) Identification of insect-damaged wheat kernels using short-wave near-infrared hyperspectral and digital colour imaging. Comput Electron Agric 73(2):118–125

107. Siripatrawan U, Makino Y (2015) Monitoring fungal growth on brown rice grains using rapid and non-destructive hyperspectral imaging. Int J Food Microbiol 199:93–100
108. Siripatrawan U, Makino Y, Kawagoe Y, Oshita S (2010) Near infrared spectroscopy integrated with chemometrics for rapid detection of *E. coli* ATCC 25922 and *E. coli* K12. Sens Actuators B Chem 148(2):366–370
109. Siripatrawan U, Makino Y, Kawagoe Y, Oshita S (2011) Rapid detection of *Escherichia coli* contamination in packaged fresh spinach using hyperspectral imaging. Talanta 85:276–281
110. Suthiluk P, Saranwong S, Kawano S, Numthuam S, Satake T (2008) Possibility of using near infrared spectroscopy for evaluation of bacterial contamination in shredded cabbage. Int J Food Sci Technol 43:160–165
111. Tallada J, Nagata M, Kobayashi T (2006) Non-destructive estimation of firmness of strawberries (*Fragaria x ananassa* Duch.) using NIR hyperspectral imaging. Environ Control Biol 44(4):245–255
112. Tao F, Peng Y, Li Y, Chao K, Dhakal S (2012) Simultaneous determination of tenderness and *Escherichia coli* contamination of pork using hyperspectral scattering technique. Meat Sci 90:851–857
113. Thanonkaew A, Benjakul S, Visessanguan W, Decker EA (2006) The effect of metal ions on lipid oxidation, colour and physicochemical properties of cuttlefish (*Sepia pharaonis*) subjected to multiple freeze–thaw cycles. Food Chem 95(4):591–599
114. Vélez N, Gómez-Sanchis J, Chanona-Pérez J, Carrasco JJ, Millán-Giraldo M, Lorente D, Cubero S, Blasco J (2014) Early detection of mechanical damage in mango using NIR hyperspectral images and machine learning. Biosyst Eng 122:91–98
115. Wang W, Heitschmidt G, Windham W, Feldner P, Ni X, Chu X (2015) Feasibility of detecting aflatoxin B1 on inoculated maize kernels surface using Vis/NIR hyperspectral imaging. J Food Sci 80(1):M116–M122
116. Wang W, Li C, Tollner EW, Gitaitis RD, Rains GC (2012) Shortwave infrared hyperspectral imaging for detecting sour skin (*Burkholderia cepacia*)-infected onions. J Food Eng 109(1):38–48
117. Wang W, Peng YK, Zhang XL (2010) Study on modeling method of total viable count of fresh pork meat based on hyperspectral imaging system. Spectrosc Spectr Anal 30(2):411–415
118. Weinstock BA, Janni J, Hagen L, Wright S (2006) Prediction of oil and oleic acid concentrations in individual corn (*Zea mays* L.) kernels using near-infrared reflectance hyperspectral imaging and multivariate analysis. Appl Spectrosc 60:9–16
119. Williams P, Geladi P, Britz T, Manley M (2012) Investigation of fungal development in maize kernels using NIR hyperspectral imaging and multivariate data analysis. J Cereal Sci 55:272–278
120. Williams P, Geladi P, Fox G, Manley M (2009) Maize kernel hardness classification by near infrared (NIR) hyperspectral imaging and multivariate data analysis. Anal Chim Acta 653:121–130
121. Wold JP, Westad F, Heia K (2001) Detection of parasites in cod fillets by using SIMCA classification in multispectral images in the visible and NIR region. Appl Spectrosc 55:1025–1034
122. Wu D, Sun D-W (2013) Advanced applications of hyperspectral imaging technology for food quality and safety analysis and assessment: a review—Part I: Fundamentals. Innov Food Sci Emerg Techol 19:1–14
123. Wu D, Sun D-W (2013) Potential of time series-hyperspectral imaging (TS-HSI) for non-invasive determination of microbial spoilage of salmon flesh. Talanta 111:39–46
124. Xie C, Wang Q, He Y (2014) Identification of different varieties of sesame oil using near-infrared hyperspectral imaging and chemometrics algorithms. PLoS One 9(5):e98522
125. Xing J, Bravo C, Jancsok PT, Ramon H, De Baerdemaeker J (2005) Detecting bruises on "golden delicious" apples using hyperspectral imaging with multiple wavebands. Biosyst Eng 90(1):27–36
126. Xing J, Hung PV, Symons S, Shahin M, Hatcher D (2009) Using a short wavelength infrared (SWIR) hyperspectral imaging system to predict alpha amylase activity in individual Canadian western wheat kernels. Sens Instrum Food Qual Saf 3:211–218
127. Xiong Z, Sun D-W, Pu H, Zhu Z, Luo M (2015) Combination of spectra and texture data of hyperspectral imaging for differentiating between free-range and broiler chicken meats. LWT Food Sci Technol 60(2):649–655
128. Xiong Z, Sun D-W, Xie A, Han Z, Wang L (2015) Potential of hyperspectral imaging for rapid prediction of hydroxyproline content in chicken meat. Food Chem 175:417–422
129. Xiong Z, Sun D-W, Xie A, Pu H, Han Z, Luo M (2015) Quantitative determination of total pigments in red meats using hyperspectral imaging and multivariate analysis. Food Chem 178:339–345
130. Yang C-C, Chao K, Chen Y-R, Early HL (2005) Systemically diseased chicken identification using multispectral images and region of interest analysis. Comput Electron Agric 49:255–271
131. Yao H, Hruska Z, Brown RL, Cleveland TE (2006) Hyperspectral bright greenish-yellow fluorescence (BGYF) imaging of aflatoxin contaminated corn kernels. Proc SPIE 6381:63810B-1–63810B-8
132. Yoon SC, Lawrence KC, Smith DP, Park B, Windham WR (2008) Embedded bone fragment detection in chicken fillets using transmittance image enhancement and hyperspectral reflectance imaging. Sens Instrum Food Qual Saf 2:197–207
133. Zhang H, Paliwal J, Jayas DS, White NDG (2007) Classification of fungal infected wheat kernels using near-infrared reflectance hyperspectral imaging and support vector machine. Trans ASABE 50(5):1779–1785
134. Zhang W, Pan L, Tu S, Zhan G, Tu K (2015) Non-destructive internal quality assessment of eggs using a synthesis of hyperspectral imaging and multivariate analysis. J Food Eng 157:41–48
135. Zhao J, Vittayapadung S, Chen Q, Chaitep S, Chuaviroj R (2009) Non-destructive measurement of sugar content of apple using hyperspectral imaging technique. Maejo Int J Sci Technol 3(1):130–142